

Water Rise in A Cellulose Foam: by Capillary or Diffusional Flow?

Morad Mirzajanzadeh, Vikram S. Deshpande, Norman A. Fleck*

Engineering Department, Cambridge University, Trumpington Street, Cambridge CB2 1PZ, UK

Abstract

Critical experiments and predictive models reveal that water rise through a cellulose foam is initially by capillary rise, followed by non-linear diffusion in the presence of trapping sites. Classical ideas on capillary rise are supported by observations that the Washburn law is obeyed up to the Jurin height. However, water rise continues beyond the Jurin height, and this subsequent phase is diffusion-controlled according to the following evidence: the nature of the quantitative dependence of water rise upon time, the insensitivity of water rise to the direction of gravity, and the fact that the water front continues to rise in the foam after the water reservoir has been removed. Water diffusion occurs through the cellulose fibre network, along with trapping/de-trapping at molecular sites. The diffusion equations are solved numerically, and, upon comparing the predictions with the observed response, values are obtained for the diffusion constant and for the ratio of trap density to lattice density. The diffusion model explains why the drying of a damp foam is a slow process: the emptying of filled traps requires diffusion through an adjacent lattice of low water content.

(keywords: foams, diffusion, computed tomography)

1. Introduction

Rising damp is ubiquitous in porous materials ranging from bricks and concrete to fibre-based materials such as wood, mineral wool insulation and cotton fabrics. A quantitative understanding of the transport of water through porous media such as cellulose is needed in

*Corresponding author at: Cambridge University Engineering Department, Trumpington St., Cambridge CB2 1PZ, UK
E-mail address: naf1@eng.cam.ac.uk (N.A. Fleck).

several industries such as textile, fabric design, printing technology, food processing, timber construction and the paper industry. In broad terms, the mechanism of liquid transport involves capillary rise and/or diffusion, but the precise details are lacking due to a paucity of appropriate experiments. This is in part due to a lack of suitable experimental techniques: only recently has it become possible to scan the distribution of water content through the thickness of these materials by micro Computed Tomography (CT), for example. And, in part, it is only recently that predictive maps have been constructed to characterise the regimes of diffusion in the presence of traps, see for example Raina et al. (2017). The current study of water migration within a cellulose foam makes use of both these experimental and theoretical advances in order to elucidate the mechanics of this commonly observed, but imperfectly understood, phenomenon.

Consider the simple experiment of placing the bottom surface of a dry cellulose foam into a reservoir of water. Initially, water rises into the foam such that the height of the advancing wet front h scales with time t according to $h \propto t^{1/2}$, then the dependence of h upon t changes to a new power law that is close to $h \propto t^{1/4}$, see for example Siddique et al. (2009). The initial phase is consistent with *either* a diffusion law, *or* capillary flow in accordance with the well-known Washburn equation¹. The Washburn equation predicts $h \propto t^{1/2}$ initially, followed by arrest of the liquid front at the so-called Jurin height. The subsequent phase of liquid rise must involve a different mechanism in order to give the observed response of $h \propto t^{1/4}$. For example, Kim et al. (2017) assume that this second regime is associated with Darcy flow through a porous media such that the permeability varies with height. Ha et al. (2018) invoked the same assumption in order to obtain the observed response of $h \propto t^{1/5}$. It is difficult to justify this

¹ Also known as the Bell-Cameron-Lucas-Washburn (BCLW) equation, as explained by Reyssat et al. (2008).

assumption on physical grounds for a uniform, homogeneous foam, and an alternative explanation is advanced in the present study.

1.1 Capillary rise

Porous materials comprise a heterogeneous network of interconnected channels, giving a physical basis for idealising liquid flow in a porous media by flow in a capillary tube. Upon neglecting inertial forces (Fries, 2008) and upon assuming a fixed contact angle between the liquid and the solid surfaces, liquid flow in a capillary tube can be derived using the Hagen-Poiseuille flow law by considering the following thought-experiment. A vertical capillary tube of uniform diameter d is brought into contact with liquid at its bottom end (see Fig. 1a). Liquid enters the tube due to suction on the liquid side of the meniscus, and gives rise to a rising height $h(t)$ of the liquid column as a function of time t . Write ω as the contact angle, γ the liquid-air surface tension, η the liquid viscosity, ρ the liquid density and g the acceleration due to gravity. Then, the net pressure drop along the tube is of magnitude $(4\gamma \cos \omega / d) - \rho gh$ and drives Poiseuille flow such that

$$\frac{4\gamma \cos \omega}{d} - \rho gh = \frac{32\eta h \dot{h}}{d^2}. \quad (1)$$

with solution

$$h + \frac{4\gamma \cos \omega}{\rho gd} \ln \left[1 - \frac{\rho gd}{4\gamma \cos \omega} h \right] = -\frac{\rho gd^2}{32\eta} t, \quad (2)$$

as first given by Washburn (1921). Note that this is also the solution for Darcy flow (Darcy, 1856) in a porous medium, upon taking the permeability κ of the porous medium to be $\kappa = d^2/32$ in terms of a representative pore diameter d . As $t \rightarrow 0$, (2) simplifies to

$$h = (\gamma d \cos \omega / 4\eta)^{1/2} t^{1/2}, \quad (3)$$

whereas as $t \rightarrow \infty$, $h(t)$ asymptotes to the limiting value

$$h = h_j = \frac{4\gamma \cos \omega}{\rho g d}, \quad (4)$$

which is known as the Jurin height (Jurin, 1717), h_j . We note that (3) is the solution to (1) in the absence of gravity, $g = 0$, and consequently (3) is the solution for horizontal capillary flow; for such horizontal flow, the Jurin height is unbounded, and capillary rise continues with increasing time, as sketched in Fig. 1b.

1.2 Diffusion

An alternative mechanism for water seepage in a porous solid is diffusion. The driving force is now the concentration C of the water in the porous solid, and the simplest diffusion law is the linear Fick's law:

$$\frac{\partial C}{\partial t} = D \frac{\partial^2 C}{\partial x^2}, \quad (5)$$

in terms of a diffusion constant D .

Consider again the simple experiment of placing the bottom surface ($x=0$) of a dry cellulose foam into a reservoir of water, and treat the foam as a half-space over $x > 0$, where x is in the vertical direction. Assume that $C(x \geq 0, t = 0) = 0$ is the initial concentration profile and enforce $C = C_0$ at $x = 0$ for $t > 0$. Then the solution of (5) is simply $C = C_0 \operatorname{erfc} \frac{x}{2\sqrt{Dt}}$ and this implies that C attains the value $C = 0.157C_0$ at the location $x = 2\sqrt{Dt}$, for example. Thus, the diffusion front migrates in the same manner as the initial stage of the Washburn equation, making it impossible to distinguish between the two mechanisms of water migration solely on the basis of the movement of the water front. However, for most practical purposes, the diffusive transport of water along a vertical foam column does not arrest at a Jurin height and this will serve as one of the methods to distinguish between the two regimes. To understand the

limitation (if any) placed by gravity on diffusive transport, recall that the chemical potential of water with a concentration C at a height h in the foam is given by

$$\mu = \mu_0 + RT \ln C + \rho_m g h, \quad (6)$$

where $\rho_m = 18 \text{ g mol}^{-1}$ is the molar density of water, R the gas constant and T the absolute temperature while μ_0 is a reference potential and g the acceleration due to gravity. Then at equilibrium, the water concentration at a height h for a given concentration C_0 at $h = 0$ is given by

$$\frac{C}{C_0} = \exp\left(-\frac{\rho_m g h}{RT}\right). \quad (7)$$

Thus, at $T = 300 \text{ K}$ the concentration $C = C_0 / e \approx 0.37C_0$ at a height $h = RT / (\rho_m g) \approx 13 \text{ km}$. Of course, this analysis is unrealistic as the acceleration due to gravity and temperature are not constant over such a large height but it serves to illustrate the point that vertical transport by diffusion is essentially unhindered by gravity for any practical laboratory experiment. Thus, the existence of a Jurin height is strong evidence for capillary rise rather than for diffusion.

The above diffusion theory neglects the presence of traps for the diffusing fluid. Now assume that traps exist: the total concentration of water is $C_{\text{TOT}} = C_L + C_T$, where $C_L(x,t)$ and $C_T(x,t)$ are the lattice and trapped water concentrations, respectively (here we are using terminology of solid state diffusion with lattice water referring to water that is weakly adsorbed by the cellulose while trapped water is the strongly adsorbed water). The diffusion equation (5) is modified to

$$\frac{\partial C_L}{\partial t} + \frac{\partial C_T}{\partial t} = D_L \frac{\partial^2 C_L}{\partial x^2}. \quad (8)$$

Here, $D_L = D_0 \exp(-Q/RT)$ is the lattice diffusion coefficient in terms of temperature T , universal gas constant R , lattice activation energy Q , and the diffusion pre-exponential factor D_0

. Introduce the trap and lattice occupancy fractions as θ_L and θ_T , respectively, such that $0 \leq \theta_L \leq 1$ and $0 \leq \theta_T \leq 1$. Then, we can write the lattice and trap concentrations as $C_L = \theta_L N_L$ and $C_T = \theta_T N_T$, respectively, where N_L is the number of lattice sites per unit volume, and N_T is the number of trap sites per unit volume. For simplicity, assume that each lattice site and each trap site can accommodate only one water molecule, and define the trap density ratio as $\bar{N} = N_T / N_L$. Equation (8) can then be rewritten as

$$\frac{\partial \theta_L}{\partial t} + \bar{N} \frac{\partial \theta_T}{\partial t} = D_L \frac{\partial^2 \theta_L}{\partial x^2}. \quad (9)$$

It remains to specify an evolution law for the trapped water. Assuming local equilibrium between the lattice sites and trapped water due to the rapid jumping of water molecules back and forth between the neighbouring lattice and trap sites (Oriani, 1970; Raina et al., 2017) we have

$$\frac{\theta_T}{1 - \theta_T} = \frac{K \theta_L}{1 - \theta_L}, \quad (10)$$

where the equilibrium constant K scales with the trap binding energy ΔH according to

$$K = \exp \left\{ \frac{-\Delta H}{RT} \right\}. \quad (11)$$

Now, when $K \gg 1$, (10) can be approximated by

$$\theta_T = \frac{K \theta_L}{1 + K \theta_L}. \quad (12)$$

and (9) can be re-expressed as

$$\left[1 + \frac{K \bar{N}}{(1 + K \theta_L)^2} \right] \frac{\partial \theta_L}{\partial t} = D_L \frac{\partial^2 \theta_L}{\partial x^2}. \quad (13)$$

The initial state of the foam is taken to be $\theta_L(x \geq 0, t = 0) = 0$, and subsequently we enforce $\theta_L(x = 0, t > 0) = \theta_L^0 > 0$. Raina et al. (2017) developed a number of analytical solutions to (13)

depending upon the values of $(K\bar{N}, K\theta_L^0)$. For example, when $K\bar{N} \approx K\theta_L^0 \gg 1$, they find that

$\theta_L = \theta_L^0 \operatorname{erfc} \frac{x}{2\sqrt{D_L t}}$. Upon defining the diffusion front by the location at which the lattice

occupancy has risen to $\theta_L = 0.157\theta_L^0$, the diffusion front is at $x = 2\sqrt{D_L t}$, in agreement with

the location of the diffusion front absent any traps (recall the solution above to (5)). However,

we emphasise that the total concentration profile is different when traps are present: the traps

have full occupancy $\theta_T = 1$ when $\theta_L > 0^+$ (since $K \gg 1$). Thus, in the presence of traps, the

diffusion front can migrate in the same manner as the early phase of the Washburn equation,

but the concentration profile behind the front is different.

The remainder of the paper is organized as follows. First, we present reservoir-fed ‘vertical tests’ in which the bottom face of a cellulose foam specimen is placed in contact with a water reservoir. We confirm that two stages of water rise exist: stage I up to a Jurin height, followed by stage II beyond the Jurin height. Additional ‘horizontal tests’ are performed on specimens such that water flow is horizontal rather than vertical to confirm that the existence of a Jurin height in the vertical tests is due to the presence of gravity. A central challenge in our study is to provide evidence that water rise in stage I vertical tests is by capillary flow while water rise in stage II (above the Jurin height) is due to diffusion. Evidence is provided in the form of density profiles in interrupted tests, involving the use of micro computed tomography (CT). Additional insight is obtained by performing a further series of tests: upon interruption of a test, the lower portion of the specimen and water reservoir are removed and water rise within the remaining upper portion of the specimen is monitored. The cut is positioned above the Jurin height, such that the ensuing response is a modification to the stage II behaviour; on restarting the test, the new initial state comprises a concentration profile of water over a finite height of foam above the cut. These ‘post-cut’ tests reveal that water diffuses through the foam,

aided by deep traps². The above diffusion model for the case of deep traps is compared to the observed water rise in the post-cut tests and in stage II of the reservoir-fed tests.

2. Reservoir-fed water rise experiment

2.1 Materials

Water rise tests were performed on a cellulose foam³ comprising a viscose cellulose matrix (dissolved cellulose of wood pulp) reinforced by cellulose fibres (Märtson, et al., 1999). Viscose, cellulose fibres, and sodium sulphate crystals were mixed mechanically and then heated to 90 – 95 °C such that the sodium sulphate melts and drains from the container leaving pore spaces in the foam (Coda, 2005). The cellulose foam has a density $\rho_f = 50 \text{ kg m}^{-3}$ and, upon assuming that the cellulose is of density $\rho_s = 1500 \text{ kg m}^{-3}$, the relative density of the foam (in the dry state) is $\bar{\rho} = 0.03$.

Scanning Electron Microscope (SEM) images of the dry cellulose foam show two scales of porosity: macropores with dimensions on the order of a few millimetres (see Fig. 2a) and micropores in the cell walls of the macropores, on a length scale on the order of a few microns (compare Figs. 2a and 2c). In the images, the label RD defines the Rise Direction of the foam.

2.2 Reservoir-fed test method

Water front advancement in cellulose foam is tracked visually, see Fig. 2d. The tests were performed using distilled water at room temperature (22 °C) such that the water-air surface tension is $\gamma = 72 \times 10^{-3} \text{ N m}^{-1}$, water density is $\rho = 1000 \text{ kg m}^{-3}$ and water viscosity is $\eta = 0.9 \times 10^{-3} \text{ Pa s}$. The time-dependent position of the wet front was recorded by a high-speed camera

² This is analogous to the diffusion of hydrogen through a metallic alloy with the diffusion aided by the presence of hydrogen traps in the microstructure.

³ Supplied by Suvic Products Ltd., 3 Brunel Rd, Totton, Southampton SO40 3WX. <http://www.suvic.co.uk/>

(frame rate in the range $25 - 100 \text{ s}^{-1}$) in the initial stage I regime of water rise, and by a CMOS camera (frame rate in the range $0.5 - 2 \text{ min}^{-1}$) in the subsequent stage II regime of water rise.

Each experiment was initiated by bringing the bottom face of the foam into contact with a reservoir of distilled water. The water level of the reservoir was maintained by the addition of water to the reservoir during each test. Two types of test were designed: *vertical* reservoir-fed tests V(RF) and *horizontal* reservoir-fed test H(RF) in order to explore the role of gravity, see Fig. 3. All tests were performed such that the Rise Direction (RD) of the foam is transverse to the water flow direction. A series of preliminary tests revealed that the water rise dynamics has a negligible sensitivity to the rise direction of the foam in relation to the water-rise direction.

Vertical Reservoir-Fed tests V(RF)

In the Vertical Reservoir-Fed tests V(RF), dry foam samples of square cross-section $w \times w$ ($w = 22 \text{ mm}$) and length 200 mm were employed, unless otherwise stated. The water front height $h(t)$ was measured from the water level of the reservoir, see Fig. 3a. The foam specimens were located inside a transparent PMMA tube (of inner diameter 38 mm) such that the bottom edge of the tube was placed inside the liquid reservoir and the top of the tube was covered by a plastic film containing a central hole of diameter 1 mm to minimize the effect of water evaporation from the sample; the PMMA tube is not included in the sketch Fig. 3a for the sake of clarity.

Horizontal Reservoir-Fed tests H(RF)

The geometry of the specimen in the Horizontal Reservoir-Fed test H(RF) is given in Fig. 3b: the specimens had a cross-section $w \times w$ ($w = 22 \text{ mm}$) and a length of 400 mm in the water-rise, X -direction. The left-hand portion of the specimen was placed in the water reservoir while the weight of the right-hand portion was supported (not shown in sketch Fig. 3b). In the H(RF) test the measurement of wet-front migration began when the wet front reached the step

in geometry (i.e. at $X = 0$) along the trajectory shown in Fig. 3b; the time required for the wet front to reach $X = 0$ and the trajectory length between this location and the reservoir were added to the measured time and wet front length, respectively.

2.3 Reservoir-fed test results

The measured wet front height h versus time t for the reservoir-fed experiments are shown in Fig. 4a. The V(RF) tests reveal two stages of water rise: stage I in support of the classical Washburn law (2), such that $h \propto t^{1/2}$ for the initial 10 seconds followed by a slower rate of rise (for $h > h_j \approx 24$ mm). In contrast, the H(RF) tests reveal that, in the absence of gravity, the rate of water rise throughout the test follows the same power law, $h \propto t^{1/2}$, as that observed in the initial phase of stage I of the V(RF) test. This is again consistent with the prediction (2) of the Washburn law absent gravity, $g \rightarrow 0$. Thus, we argue that $h_j = 24$ mm in the vertical test is the Jurin height for capillary rise.

Now consider stage II of water rise (that is, beyond the Jurin height) for the V(RF) tests. We note in passing that the dependence of $h(t)$ over the full range of time t in stage II of water rise does not support a single power law fit. Initially, soon after the Jurin height has been achieved we find that $h \propto t^{1/5}$ as suggested by Ha et al. (2018) whereas the data over the full span of the stage II can be fitted by the relation of the form $h \propto t^{1/4}$, although it has no obvious physical basis; recall the study by Siddique et al. (2009) and by Kim et al. (2017). It is instructive to assume that the second regime of water-rise initiates when the Jurin height is attained. Accordingly, rescale $h(t)$ to $h'(t')$ where $h' \equiv h - h_j$ and $t' \equiv t - t_j$, where t_j is the time to attain the point of inflection on the $h(t)$ curve, that is, the time to attain the Jurin height h_j . The replot $h'(t')$ of the data is shown in Fig. 4b for the V(RF) tests: we note that $h' \propto t'^{1/2}$, indicative of either diffusion or capillary flow. Now, if stage II is also due to capillary flow,

then we would anticipate the existence of a second Jurin height associated with finer capillaries than in Stage I. In order to explore whether a second Jurin height exists in stage II, a test was continued for about 6 days using a specimen of length 400 mm; no second Jurin height was observed (see Fig. 4a). It proved impractical to continue the experiments for a longer period due to the effects of water evaporation. An alternative strategy was adopted to distinguish between diffusion and capillary rise: we measured the density profile within the foam in a post-cut V(RF) test in order to distinguish between water rise by capillary flow and by diffusion.

2.4 Density profile

The spatial distribution of foam density was measured by micro computed tomography (CT) after interruption of a series of nominally identical vertical reservoir-fed test V(RF). Checks were made on the accuracy of the CT measurements by performing additional destructive tests whereby the specimen was cut into transverse slices and the density of each slice was measured via its weight and volume. The computed tomography x-ray scans were performed using a 50 kV x-ray source, a 1s exposure time and a spatial resolution of 36 μm per voxel unit: this is the highest achievable resolution as dictated by the dimension of the foam specimens and the performance of the CT machine⁴.

Each scan of the V(RF) foam samples takes about one hour, and, in order to prevent migration of water along the foam specimen during the measurement, the foam samples were frozen at the desired instant during the V(RF) test, and maintained in the frozen state during the CT scan. The procedure was as follows. When the wet front attained the desired position in the vertical reservoir-fed V(RF) test, the foam sample was quickly removed from the water reservoir and immersed in liquid nitrogen. In order to avoid infiltration of the foam by liquid nitrogen, the foam was sheathed in a thin film of low density polyethylene (LDPE) immediately

⁴ Nikon X-TEK (XT H 225ST) machine. Post-processing analysis of the reconstructed CT images was performed using VGStudio MAX 2.2 software.

prior to immersion. The foam was maintained in the frozen state during the CT scan by suspending it above a bath of liquid nitrogen during the CT scans: the temperature of the foam was maintained below $-70\text{ }^{\circ}\text{C}$ by this arrangement. In order for the foam samples to fit into the CT machine (and maximise resolution), the samples were cut into 45 mm lengths after being frozen. The foam density profile was measured in slices of thickness 1mm (along the height of the foam column) by the post-processing CT software following the calibration of the CT scan results against the density of the distilled water, i.e. 1000 kg m^{-3} . The average foam density at each slice is calculated via the rule of mixtures by measuring the volume fraction and mean density value of the foam and water from a calibrated density histogram of each slice.

2.5 Results and discussion for the foam density measurement of V(RF) tests

Representative CT images of the cellulose foam after the V(RF) test in Fig. 5a shows the distribution of water at the mid-plane section of the foam. The density distribution of the foam during the V(RF) tests, at selected times, is shown in Fig. 5b. We make the following deductions: (i) within stage I of water rise, the foam density attains a steady state profile, and (ii) within stage II of water rise, the foam density profile spreads along the foam with increasing time. Now compare the measured profile with the predictions of the Washburn theory of capillary rise, and of diffusion theory. The Washburn prediction of density for an array of identical capillary tubes gives a uniform density profile in stage I of water rise, as sketched in Fig. 6a; this is qualitatively different from that observed in Fig. 5b. One approach is to interpret the non-uniform density profile, as observed in our tests, as evidence that the foam microstructure behaves as an ensemble of capillary tubes of varying diameter, as sketched in Fig. 6b. But, the evolving density profile in stage II of the V(RF) tests (Fig. 5b) suggests diffusional flow, and we proceed to provide further evidence for this via a series of additional experiments.

3. Post-cut liquid rise experiments

Capillary rise requires the existence of a fluid reservoir to feed the capillaries. If such a reservoir were removed, then capillary rise would arrest immediately. This motivates a second set of experiments, such that the liquid reservoir is removed by making a cut in the foam column near the Jurin height and then by removing the wet foam below the cut height. This critical experiment is detailed here. Two types of test were performed: the vertical post-cut test V(PC) and the horizontal post-cut test H(PC).

The vertical post-cut V(PC) test

The vertical post-cut V(PC) test setup is sketched in Fig. 7a; it was performed as follows. First, a V(RF) test was conducted until the wet front length h had extended to a selected distance $h(t_c)$ at a time t_c beyond the Jurin height, h_j . The specimen was then removed from the water reservoir and the sample was cut across its cross-section at a height h_c into two pieces, such that h_c is intermediate between $h(t_c)$ and the Jurin height h_j . The wet length of the specimen above the cut is $l_c = h(t_c) - h_c$, and provides a source of water migration along the remaining dry portion of the specimen beyond the height $h(t_c)$. The test was resumed such that the rescaled wet front height $\hat{h} = h - h_c$ was measured as a function of time $\hat{t} = t - t_c$.

The horizontal post-cut V(PC) test

The horizontal post-cut specimen H(PC) is shown in Fig. 7b. The preparation of the specimen is identical to that for the V(PC) test; the only difference is that, after the specimen has been cut at the height h_c , the upper portion is rotated to the horizontal direction and the wet front length $\hat{h} = h - h_c$ was measured as a function of rescaled time $\hat{t} = t - t_c$.

3.1 Results and discussion for the post-cut tests

Typical $h(t)$ responses from the V(PC) and H(PC) post-cut tests are plotted on Fig. 8, for the choice $h_C = h_J = 24$ mm and $l_C = 44$ mm. In addition, the responses for the reservoir-fed tests V(RF) and H(RF) are included on the plot. A number of deductions can be made, as follows.

- (i) The direction of gravity (relative to the axis of the specimen) does not affect the rate of water migration in the V(PC) and H(PC) tests. This is consistent with the predictions of diffusion theory, or alternatively, with the early stages of capillary flow.
- (ii) The post-cut $h(t) > h_C$ response in the V(PC) and H(PC) tests is identical to that in stage II of the vertical reservoir-fed test V(RF). This is suggestive of diffusional flow.
- (iii) Arrest of the wet front is observed for both the V(PC) and H(PC) tests at $t = t_K = 3 \times 10^4$ s: this appears as a *knee* in the plot of Fig. 8. The dependence of the wet front height (at the knee) upon h_C and l_C is summarised in Table 1. Arrest of the diffusion front in the post-cut V(PC) and H(PC) tests is suggestive of water transport by diffusion in the presence of deep traps.

Additional insight into the transport mechanism in stage II is obtained by measurement of density profiles of frozen specimens by CT scans (using the same method as that described for the reservoir-fed tests). Representative density profiles are shown in Fig. 9 for the vertical post-cut test V(PC), for the choice $h_C = h_J = 24$ mm and $l_C = 24$ mm. Profiles are shown immediately after making the cut ($\hat{t} = 0$), at an intermediate time $\hat{t} = 800$ s, and at the *knee* ($\hat{t} = \hat{t}_K = 10^4$ s). The observed density profile, and the presence of the knee in the $\hat{h}(\hat{t})$ response supports an

interpretation of diffusion in the presence of deep traps as follows. We infer from Fig. 9 that, at time $\hat{t} = 0$, the lattice occupancy fraction θ_L varies almost linearly from a value of θ_L^J at the Jurin height to a value of zero at the wet front. Take the traps to be deep such that $K \gg 1$ and refer to (12); then, the occupancy fraction of traps θ_T equals unity if $\theta_L > 0$ and vanishes if $\theta_L = 0$, as sketched in Fig. 10a. Write ξ as the axial co-ordinate beyond the cut, and recall that the distance from the cut to the position of the wet front at $\hat{t} = 0$ is written as l_C . Then, upon writing θ_L^* as the lattice occupancy fraction at the cut (above the Jurin height), we have $\theta_L(0 < \xi < l_C, \hat{t} = 0) = \theta_L^*(1 - \xi/l_C)$ and $\theta_T(0 < \xi < l_C, \hat{t} = 0) = 1$, see Fig. 10a.

Full numerical solutions are given below for the diffusion equation (13) in the presence of deep traps. The qualitative nature of the solution is given now in order to show that it is consistent with the observations of the post-cut experiments as reported in Figs. 8 and 9. In broad terms, lattice diffusion leads to propagation of the wet front, with $\theta_T = 1$ behind the wet front. This process continues until the lattice occupancy θ_L drops to a sufficiently low value that θ_T drops to below unity, and the traps begin to empty again. De-trapping of the water molecules from the trap sites is sketched in Fig. 10b, and takes place at a very slow rate due to the fact that the de-trapped water must drain into a lattice for which $K\theta_L \ll 1$. This explains the knee in the $\hat{h}(\hat{t})$ response, recall Fig. 8. The detailed numerical solution is now presented to support this view.

4. Theory of water diffusion in a cellulose foam

Lattice diffusion in stage II (beyond the Jurin height) is modelled by (13), with deep traps present, as sketched in the energy landscape of Fig. 11. Recall that the regimes of solution of (13) depend upon the values of $K\theta_L^0$ and $K\bar{N}$, as discussed in detail by Raina et al. (2017).

We shall show that our observations of water migration support the notion that $K\theta_L^0 \approx K\bar{N} \gg 1$ (termed regime IIIb in Raina et al. (2017)). For example, the sharp wet front in the stage II reservoir-fed test indicates that diffusion occurs within regime III according to the classification of Raina et al. (2017)⁵. Within this regime, the diffusion front length λ advances with time t according to $\lambda \approx 2\sqrt{D_L t}$. Recall the $h'(t')$ response as shown in Fig. 4b for the V(RF) tests is of the form $h' = 2\sqrt{D_L t'}$ and we thereby obtain $D_L = 3.8 \times 10^{-7} \text{ m}^2 \text{ s}^{-1}$.

The value of the equilibrium constant K is obtained directly from the trap binding energy ΔH through equation (11). In principle, the trap binding energy between cellulose and liquid water can be calculated from the heat of absorption of liquid water by cellulose. However, an examination of the relevant literature (see below) reveals that it is difficult to measure the heat of absorption of water by cellulose at zero moisture regain, as defined by the amount of moisture present in material before absorption commences. Rees (1948) reviewed measurements of the heat of wetting and absorption of water by a range of celluloses and found that the extrapolated value for the heat of absorption at zero moisture regain is 21.3 kJ mol^{-1} , based on the measured heat of wetting data with the minimum moisture regain of 0.3%, 0.9% and 1.2%. A more precise measurement by Morrison and Dzieciuch (1959) gives the heat of absorption of liquid water by cellulose at zero moisture regain to be $31.76 \text{ kJ mol}^{-1}$, based on measured heat of wetting data with the minimum moisture regain of 0.17%. More recently, Portugal et al. (2010) has calculated a higher heat of sorption of liquid water by cellulose to be 35 kJ mol^{-1} . Here, we will take the heat of absorption of liquid water by cellulose to be $31.76 \text{ kJ mol}^{-1}$, as suggested by Morrison and Dzieciuch (1959); the equilibrium constant K follows immediately from (11)

⁵ In the regime I diffusion, diffusion front length h advance with time t through $h \propto t^{1/2}$; however, the diffusion front is not sharp for regime I.

as $K = 4.3 \times 10^5$. It remains to state the trap density \bar{N} in order to solve the governing diffusion equation (13).

4.1 Trap density

Consider again the measured foam density profiles in the vertical post-cut tests V(PC), for the case where the cut height h_c equals the Jurin height h_j , recall Fig. 9. The wet foam density at the location $h_c = h_j$, as measured immediately after making the cut $\hat{t} = 0$ and at the knee point $\hat{t} = \hat{t}_k = 10^4$ s of the h versus t curve of Fig. 8, are now used to deduce the values of N_T and θ_L^J / \bar{N} as follows. The density of the wet foam at any location $\rho(\xi, \hat{t})$ is related to the total concentration of water $C_{TOT} = \theta_L N_L + \theta_T N_T$ by

$$\rho - \rho_0 = (\theta_L N_L + \theta_T N_T) \frac{M_w}{N_A}, \quad (14)$$

where M_w is the molar mass of water molecules, N_A the Avogadro constant and ρ_0 is the dry foam density. Write θ_L^J as the lattice occupancy of water at the Jurin height at $\hat{t} = 0$, and note that $\theta_T = 1$. Then, (14) can be re-written as

$$\rho_J - \rho_0 = \left(\frac{\theta_L^J}{\bar{N}} + 1 \right) \frac{M_w}{N_A} N_T. \quad (15)$$

Also, at $\hat{t} = \hat{t}_k = 10^4$ s, it is assumed that $\theta_L = 0$ and $\theta_T = 1$ over the zone $0 \leq \xi \leq \hat{h}$, and (14) reduces to

$$\rho(0, \hat{t}_k) - \rho_0 = \frac{M_w N_T}{N_A}, \quad (16)$$

Upon taking $\rho_J = 250 \text{ kg m}^{-3}$, $\rho_0 = 50 \text{ kg m}^{-3}$ and $\rho(0, \hat{t}_k) = 85 \text{ kg m}^{-3}$ as the relevant measured densities in Fig. 9, the pair of equations (15) and (16) can be solved to give $N_T = 1.17 \times 10^{27} (\text{m}^{-3})$ and $\theta_L^J / \bar{N} = 4.71$.

Alternatively, the value of θ_L^J / \bar{N} can be determined by mass conservations of water for the times $\hat{t} = 0$ and $\hat{t} = \hat{t}_K$ as follows. Consider the more general case where $h_C \neq h_J$, as sketched in Fig. 10. Assume that the lattice occupancy of the water at $\hat{t} = 0$ varies in a linear fashion over $0 \leq \xi \leq l_C$, and write $\theta_L = \theta_L^* = \theta_L^J l_C / l_J$ at $\xi = 0$, where l_J is the length of wet foam above the Jurin height, such that $l_J = l_C + h_C - h_J$. Also assume that, at $\hat{t} = \hat{t}_K$, we have $\theta_L = 0$ and $\theta_T = 1$ over the zone $0 \leq \xi \leq \hat{h}_K$. Then, mass conservation dictates that

$$\frac{\theta_L^J}{\bar{N}} = \frac{2l_J(\hat{h}_K - l_C)}{l_C^2}. \quad (17)$$

Calculated values of θ_L^J / \bar{N} using (17) for selected post-cut tests are listed in Table. 1, giving an average value of $\theta_L^J / \bar{N} = 4.1$ from all of the tests listed in Table 1. This average is somewhat below the value $\theta_L^J / \bar{N} = 4.71$ as deduced by the previous method, and since we are unable to state that one method is more accurate than the other, we adopt the pragmatic approach of taking the overall average to be $\theta_L^J / \bar{N} = 4.4$. We shall show subsequently via numerical calculations, see Fig. 12, that $\theta_L^J = 0.1$ gives good agreement with measurements and thus we infer a value of $\bar{N} = 0.02$. This implies that with $N_T = 1.17 \times 10^{27} \text{ m}^{-3}$, the lattice site density $N_L = 51.5 \times 10^{27} \text{ m}^{-3}$.

5. Numerical analysis of the post-cut (PC tests)

We assume the following material parameters for the diffusion model as measured above: $K = 4.3 \times 10^5$, $N_T = 1.17 \times 10^{27} \text{ m}^{-3}$, $N_L = 51.5 \times 10^{27} \text{ m}^{-3}$ ($\bar{N} = 0.02$) and $D_L = 3.8 \times 10^{-7} \text{ m}^2 \text{ s}^{-1}$. The PDE (13) is solved numerically by using the partial differential equation solver *pdepe* in MATLAB⁶. The *pdepe* solver has an automatic time-stepping routine to ensure

⁶ <https://www.mathworks.com/>

temporal convergence. The simulations used a uniform mesh of mesh size $e = 0.1$ mm: a mesh sensitivity analysis confirm that this spatial resolution was sufficient for all cases considered.

The initial conditions and boundary conditions are as follows. Assume that the lattice occupancy fraction θ_L of water at $\hat{t} = 0$ varies linearly over $0 \leq \xi \leq l_C$, and write $\theta_L = \theta_L^*$ at $\xi = 0$. The remainder of the foam is dry, such that $\theta_L = 0$. At $\hat{t} > 0$, the water lattice occupancy is taken to be $\theta_L = 0$ at the right-hand boundary $\xi = +\infty$ while the flux $\partial\theta_L / \partial\xi$ vanishes at the left-hand boundary $\xi = 0$.

The magnitude of the initial lattice occupancy fraction at the Jurin height θ_L^J is obtained by matching numerical predictions of $\hat{h}(\hat{t})$ to the observed solution for the case $l_C = 22$ mm, see Fig. 12. Acceptable agreement is obtained by assuming that $\theta_L^J = 0.1$. Upon adopting this value for θ_L^J , numerical predictions of the spatial distribution of foam density at selected times are compared with the measured profile in Fig. 9. Good agreement is noted between predicted and measured profiles, in support of the diffusion model with deep traps.

In order to obtain further support for the diffusion model with deep traps, it is instructive to compare the predictions of the numerical model with the measured distribution of water (at lattice sites and at traps) from the vertical reservoir-fed tests, recall Fig. 5. Predictions of the density of the wet foam are in excellent agreement with the measured distributions by CT analysis.

6. Conclusions

The transport of water through a cellulose foam has been investigated through a series of critical experiments designed to reveal the operative mechanisms. These experiments strongly suggest two regimes of behaviour for the rise of water in a vertical foam under the influence of gravity. In stage I, the transport is driven by capillary forces but this mechanism

becomes non-operative above the so-called Jurin height which, in this case, is approximately 24 mm. However, water in these vertical experiments continues to rise above the Jurin height, albeit at a slower rate, now driven by a diffusive flow mediated by trapping at deep traps (i.e. sites within the foam that have a high affinity for water). Transport of water in a horizontal foam (where gravity plays no role) is always dominated by the fast capillary mechanism. Additional experiments measuring the water density (concentration) profiles within the foam at various stages of the transport as well as measurements where the water reservoir was eliminated confirmed the operation of these two distinct mechanisms.

A model for the diffusive transport of water in the cellulose foam in the presence of the deep traps is also presented. Key parameters of the model including the density of the trapping sites, the trapping enthalpy and diffusion co-efficient are determined via independent measurements and comparisons of the numerical solution of the diffusion equations with observations. The water transport mechanisms, as well as the models presented, are expected to have application beyond cellulose foams. For example, rising damp in porous building materials is a problem of great practical interest, and application of the ideas of the current study (both experimental techniques and models) to such problems remain topics for future work.

Acknowledgements

The authors are grateful for financial support of this work in the form of an ERC MULTILAT grant 669764.

References

- Bell, J. M. & Cameron, F. K., 1906. The flow of liquids through capillary spaces. *The Journal of Physical Chemistry*, 10(8), pp. 658-674.
- Cambau, T., Bico, J. & Reyssat, E., 2011. Capillary rise between flexible walls. *EPL (Europhysics Letters)*, 96(2), p. 24001.
- Coda, R., 2005. *a study of cellulose based biodegradable foams and sponges*, s.l.: M.S. thesis, Georgia Institute of Technology.

Darcy, H., 1856. *Les fontaines publiques de la ville de Dijon: exposition et application...* s.l.:Victor Dalmont.

Elwinger, F., Pourmand, P. & Furo, I., 2017. Diffusive Transport in Pores. Tortuosity and Molecular Interaction with the Pore Wall. *The Journal of Physical Chemistry C*, 121(25), pp. 13757-13764.

Fries, N. D. M., 2008. The transition from inertial to viscous flow in capillary rise. *Journal of colloid and interface science*, 327(1), pp. 125-128.

Ha, J., Kim, J., Jung, Y., Yun, G., Kim, D. N., & Kim, H. Y., 2018. Poro-elasto-capillary wicking of cellulose sponges. *Science advances*, 4(3), p. eaao7051.

Jurin, J., 1717. An Account of Some Experiments Shown before the Royal Society; With an Enquiry into the Cause of the Ascent and Suspension of Water in Capillary Tubes. *Philosophical Transactions*, 30(351-363), pp. 739-747.

Kim, J., Ha, J. & Kim, H.-Y., 2017. Capillary rise of non-aqueous liquids in cellulose sponges. *Journal of Fluid Mechanics*, Volume 818.

Lucas, R., 1918. Ueber das Zeitgesetz des kapillaren Aufstiegs von Flüssigkeiten. *Colloid & Polymer Science*, 23(1), pp. 15-22.

Märtson, M., Viljanto, J., Hurme, T., Laippala, P., & Saukko, P., 1999. Is cellulose sponge degradable or stable as implantation material? An in vivo subcutaneous study in the rat. *Biomaterials*, 20(21), pp. 1989-1995.

McNabb, A. & Foster, P. K., 1963. A new analysis of the diffusion of hydrogen in iron and ferritic steels. *Trans. Metall. Soc. AIME*, 227(3), pp. 618-627.

Morrison, J. L. & Dzieciuch, M. A., 1959. The thermodynamic properties of the system cellulose-water vapor. *Canadian Journal of Chemistry*, 37(9), pp. 1379-1390.

Oriani, R. A., 1970. The diffusion and trapping of hydrogen in steel. *Acta metallurgica*, 18(1), pp. 147-157.

Portugal, I., Dias, V. M., Duarte, R. F. & Evtuguin, D. V., 2010. Hydration of cellulose/silica hybrids assessed by sorption isotherms. *The Journal of Physical Chemistry B*, 114(11), pp. 4047-4055.

Raina, A., Deshpande, V. S. & Fleck, N. A., 2017. Analysis of electro-permeation of hydrogen in metallic alloys. *Phil. Trans. R. Soc. A*, 375(2098), p. 20160409.

Raina, A., Deshpande, V. S. & Fleck, N. A., 2018. Analysis of thermal desorption of hydrogen in metallic alloys. *Acta Materialia*, Volume 144, pp. 777-785.

Rees, W. H., 1948. The heat of absorption of water by cellulose. *Journal of the Textile Institute Transactions*, 39(11), pp. T351-T367.

Reyssat, M., Courbin, L., Reyssat, E. & Stone, H. A., 2008. Imbibition in geometries with axial variations. *Journal of Fluid Mechanics*, Volume 615, pp. 335-344.

Siddique, J. I., Anderson, D. M. & Bondarev, A., 2009. Capillary rise of a liquid into a deformable porous material. *Physics of Fluids*, 21(1), p. 013106.

Washburn, E. W., 1921. The dynamics of capillary flow. *Physical review*, 17(3), p. 273.

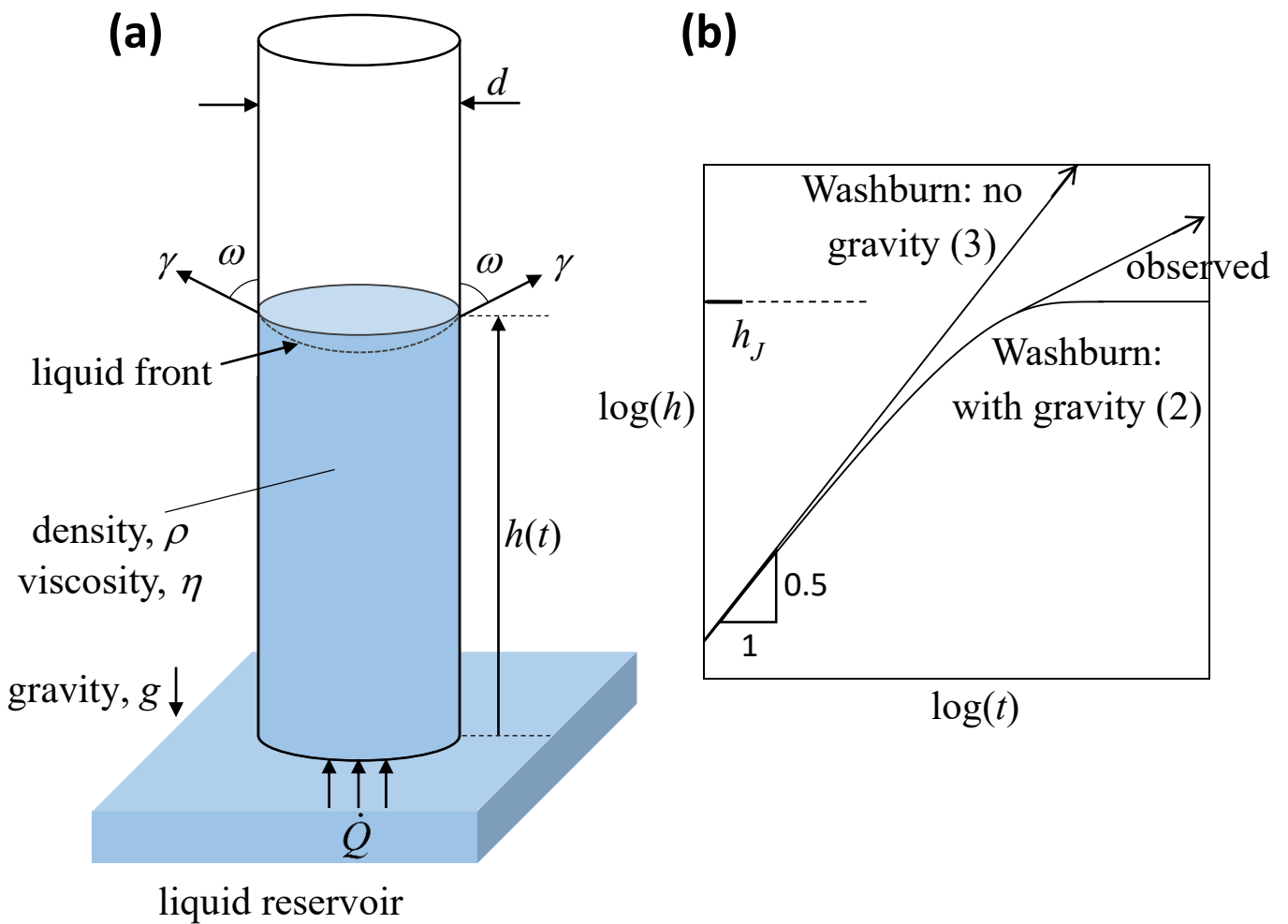


Fig. 1. (a) Sketch of capillary rise in a vertical tube. (b) Sketch of the capillary rise height versus time in the presence of gravity as given by equation (2), in the absence of gravity via equation (3), and the *observed* behaviour. The equilibrium height in the vertical capillary tube, in the presence of gravity, is the Jurin height h_J .

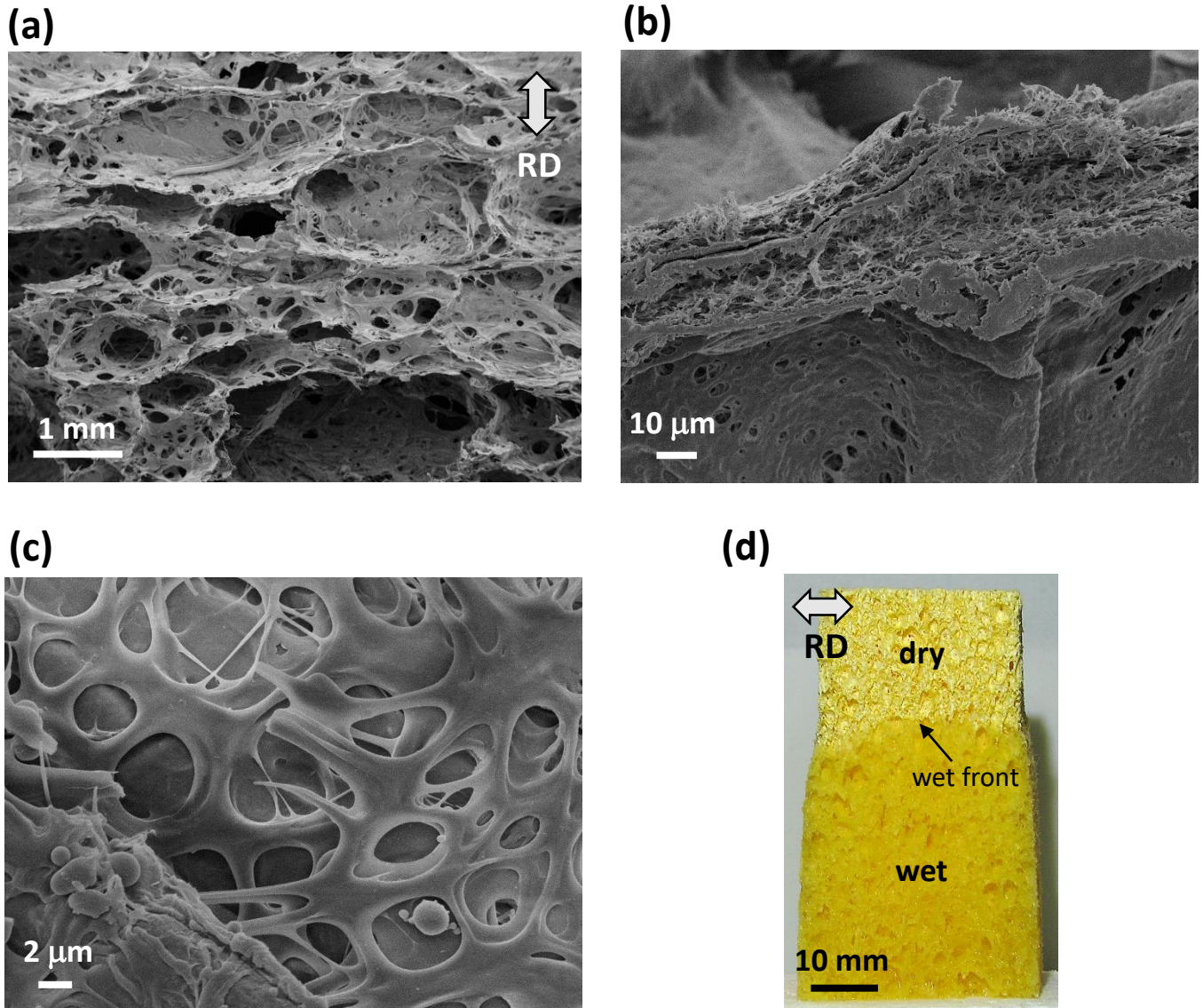


Fig. 2 (a) SEM image of the dry cellulose foam showing macropores. (b) The cell walls of the macropores are made of micropores. (c) Magnified image of the micropores. (d) Optical image of the partially wet cellulose foam. The label RD defines the Rise Direction of the foam.

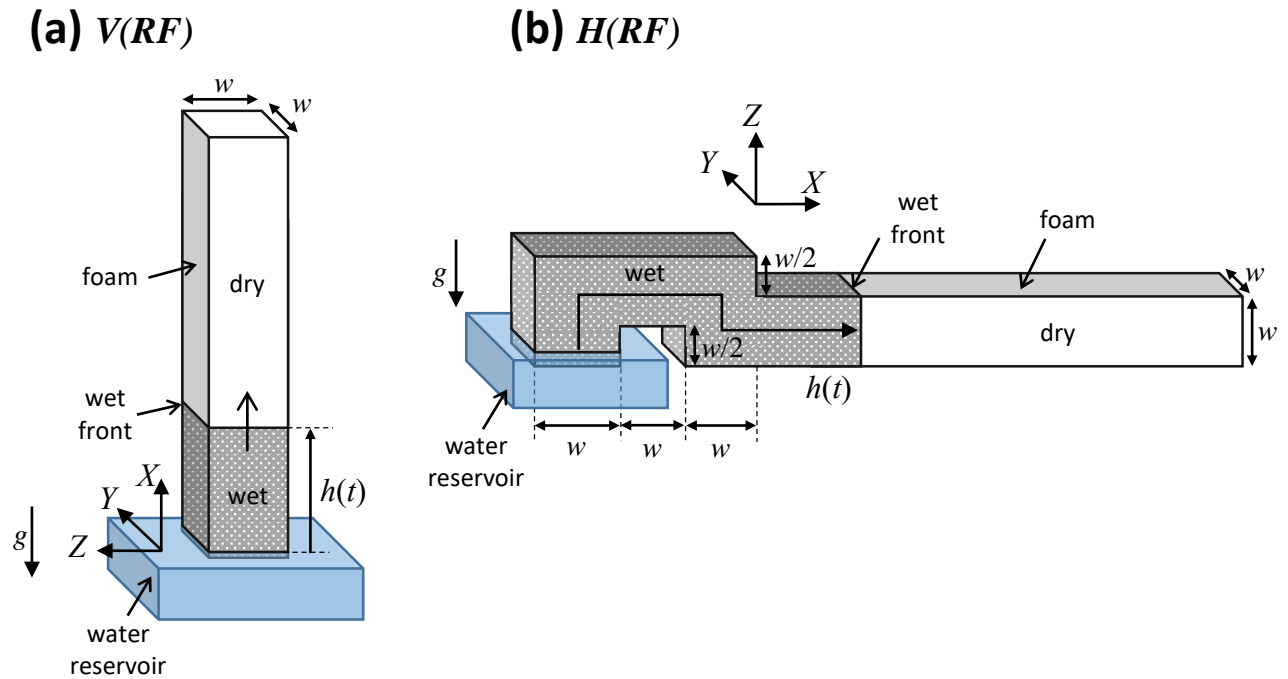


Fig. 3. (a) Test geometry for the Vertical Reservoir-Fed test V(RF): the water front height $h(t)$ is measured from the water level of the reservoir. (b) Test geometry for the Horizontal Reservoir-Fed test H(RF). The Rise Direction of the foam (RD) is in the Y -direction, as shown.

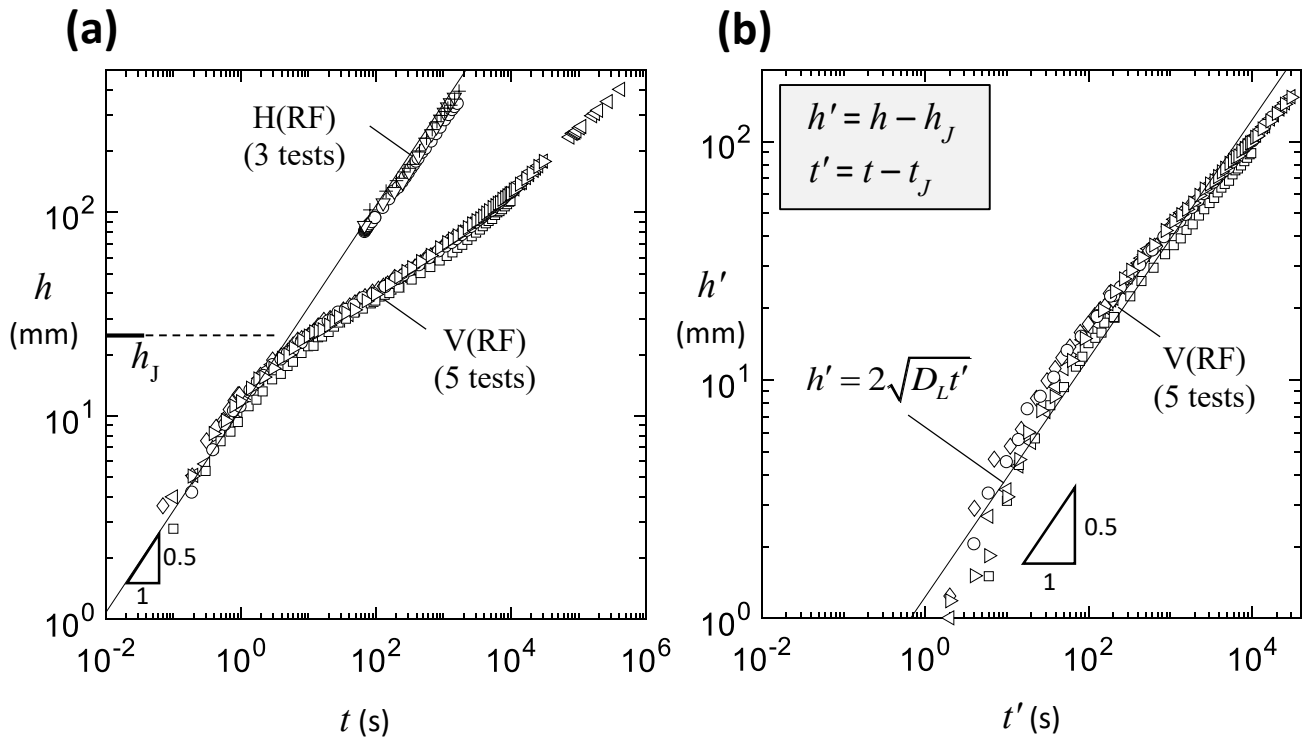


Fig. 4. (a) Measured wet front length h with time t for the vertical reservoir-fed test V(RF) and the horizontal reservoir-fed test H(RF). (b) The $h(t)$ response is replotted as $h'(t')$ where $h' = h - h_J$ and $t' = t - t_J$.

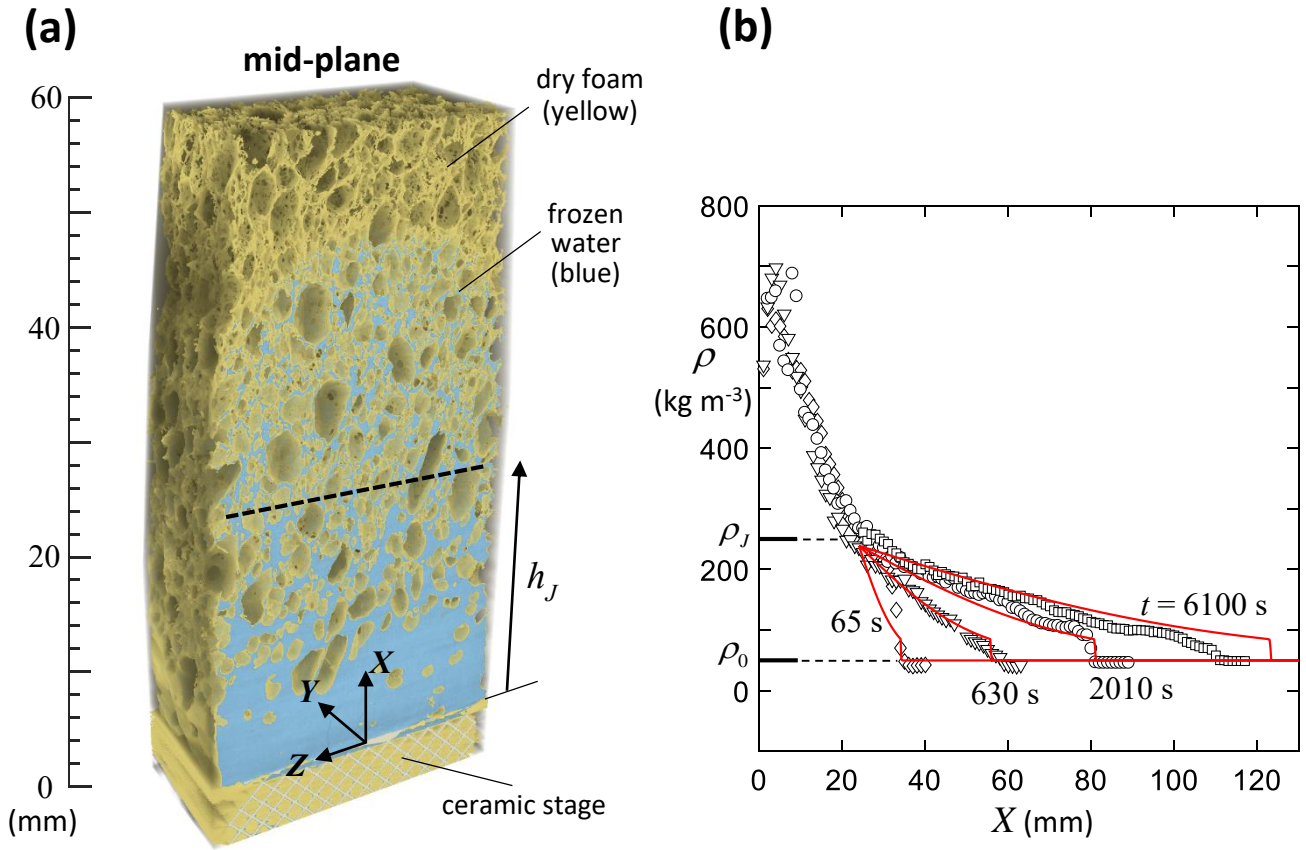


Fig. 5. (a) Representative 3D reconstructed computed tomography x-ray image of the partially wetted cellulose foam. (b) Measured foam density ρ versus position X at selected times in the vertical reservoir-fed test V(RF). Numerical predictions are included (solid lines).

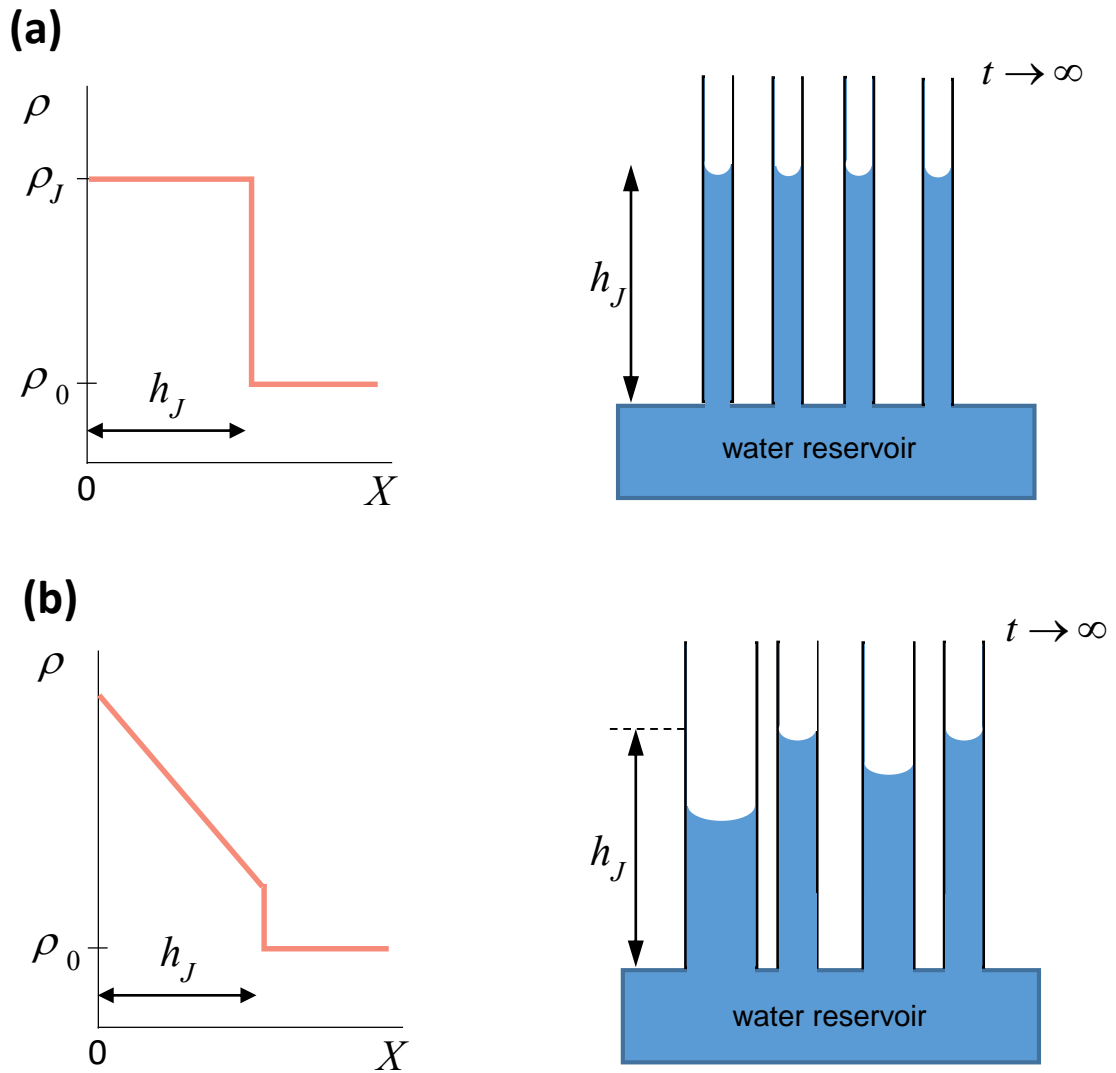


Fig. 6. (a) A sketch of the density profile as given by the Washburn prediction for an array of identical capillary tubes in stage I of water rise. (b) A sketch of the observed density profile in stage I of water rise in foam: a non-uniform distribution of ρ suggests the existence of a dispersion of capillary tube diameters. The foam density at the Jurin height is ρ_J , and the density of the dry foam is ρ_0 .

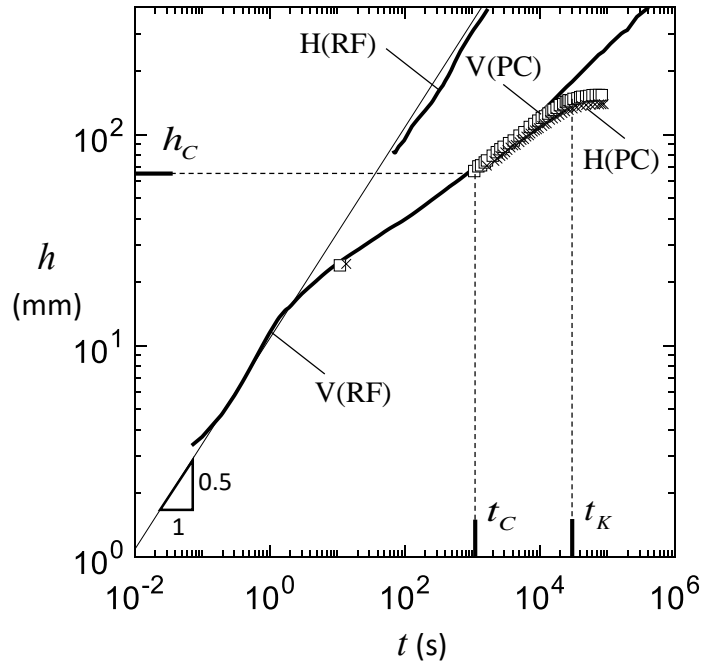


Fig. 8. A comparison of $h(t)$ for vertical and horizontal post-cut tests, V(PC) and H(PC), respectively, for the choice $h_C = h_J = 24$ mm and $l_C = 22$ mm. The measured $h(t)$ responses from reservoir-fed tests V(RF) and H(RF) are taken from Fig. 4a for comparison purposes.

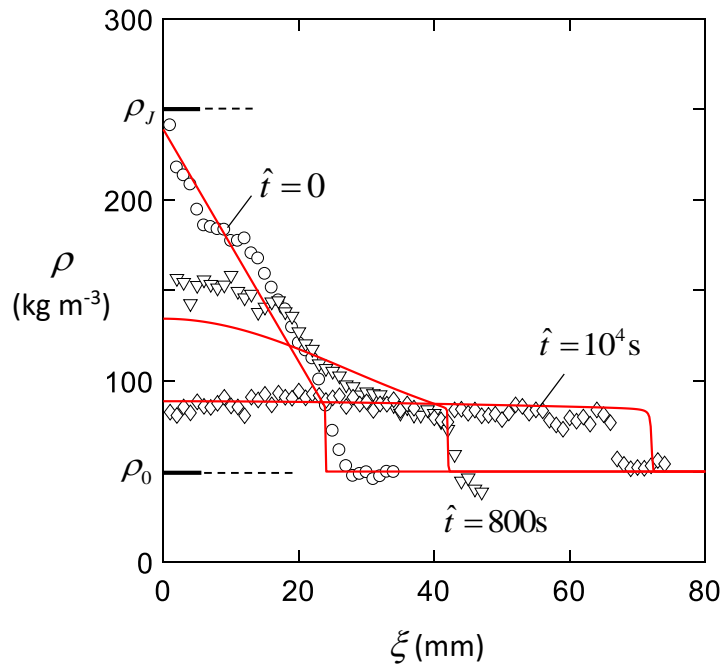
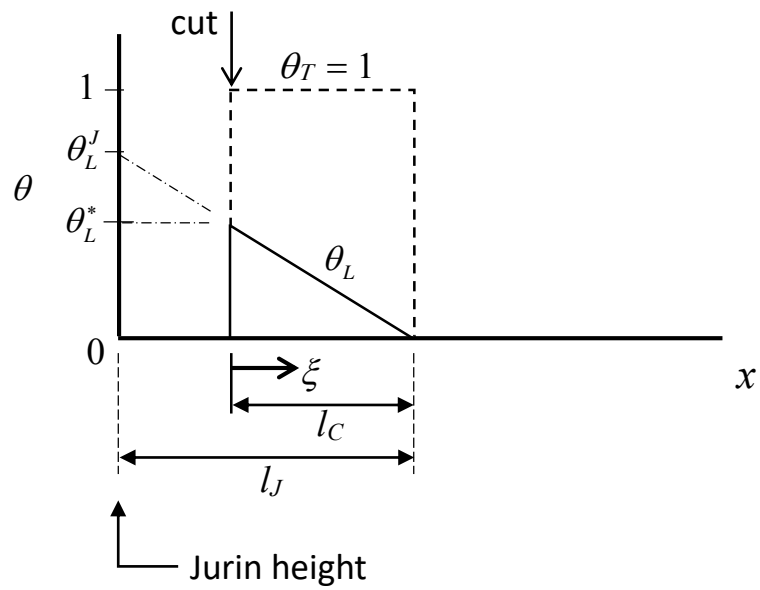


Fig. 9. The density profile $\rho(\xi)$, as measured by CT scans, for the V(PC) tests with $h_C = h_J = 24$ mm and $l_C = 24$ mm. Measurements are reported at $\hat{t} = 0$, $\hat{t} = 800$ s and at $\hat{t} = \hat{t}_K = 10^4$ s. Numerical predictions are included.

(a) at $t = t_c$ ($\hat{t} = 0$)



(b) at $\hat{t} = \hat{t}_K$

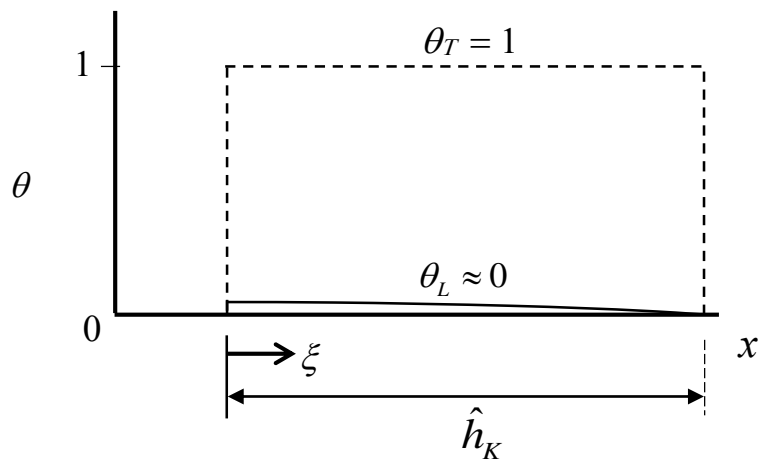


Fig. 10. Inferred profiles of (θ_L, θ_T) in the vertical post-cut tests at (a) $\hat{t} = 0$ and $\hat{t} = \hat{t}_K$.

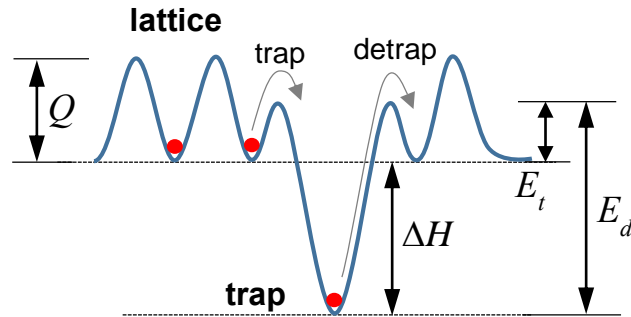


Fig. 11. A sketch of the energy landscape for the kinetics of water diffusion through the lattice and at trap sites: The activation energy barrier for diffusion through the lattice is Q , and the trapping enthalpy is ΔH . The quantities E_t and $E_d = E_t - \Delta H$ are the trapping and de-trapping energy barriers, respectively, although E_t plays no explicit role in the analysis used here assuming local equilibrium between the lattice and trapped water.

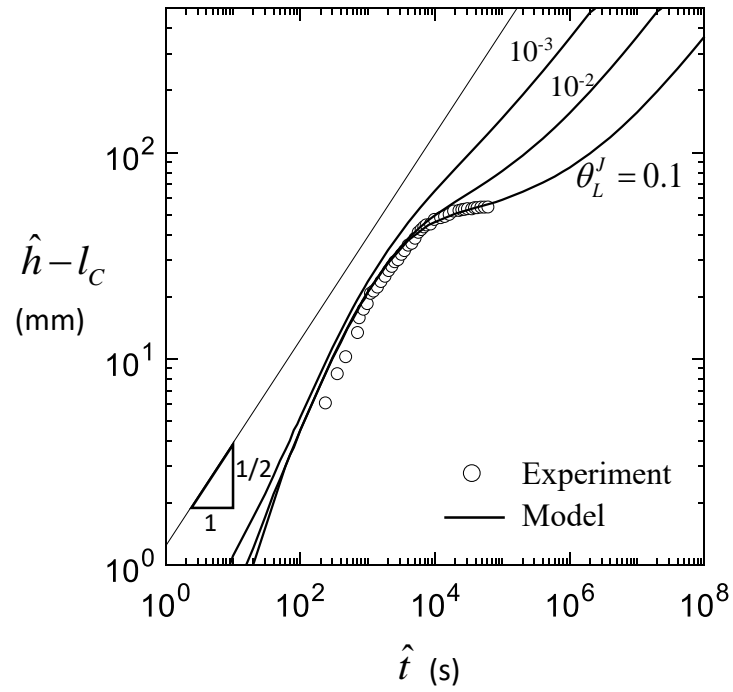


Fig. 12. Measured liquid rise \hat{h} versus time \hat{t} for the post-cut tests, for the choice $h_C = h_J = 24$ mm and $l_C = 22$ mm. Predictions by solving (13) are included for selected values of θ_L^J .

Table 1. Chosen values of (h_c, l_c) in the V(PC) tests, in relation to the Jurin height $h_J = 24$ mm.

Measured values of \hat{h}_k and deduced values of θ'_L / \bar{N} from (17) are also given.

Tests	h_c (mm)	l_c (mm)	\hat{h}_k (mm)	$\frac{\theta'_L}{\bar{N}}$
V(PC)	h_J+22	22	44	4.00
V(PC)	h_J	22	70	4.36
V(PC)	h_J	22	74	4.72
V(PC)	h_J	44	130	3.91
H(PC)	h_J	44	119	3.41